LETTERS IN HEAT AND MASS TRANSFER 0094-4548/82/020119-11$03.00/0
Vol. 9, pp. 119-129, 1982

GAS-LIQUID MASS TRANSFER IN ROTATING PERFORATED-DISC CONTACTORS

Wen-Jei Yang
University of Michigan
Department of Mechanical Engineering & Applied Mechanics
Ann Arbor, Michigan 48109

(Communicated by J.P. Hartnett and W.J. Minkowycz)

ABSTRACT

This paper presents a numerical model for predicting the performance of liquid-gas mass transfer in a rotating perforated-disc type contactor. The device consists of a cylindrical section situated between two 45-degree conical sections. A liquid flows downward by gravity while a stream of air moves upward by buoyancy thus forming a counter-current flow situation in the contactor. A gas dissolved in the liquid transfers into air bubbles which are sheared to a tiny size as they rise through the perforations on the rotating disc. Both laminar and turbulent flows are treated. Utilizing the velocity distribution [10,11] and bubble trajectory [12] as the basis, the interphase mass transfer performance of carbon dioxide in the water-air system is numerically determined. It is disclosed that in both laminar and turbulent flow cases, the rate of interphase mass transfer increases significantly with a reduction in bubble size. Rotational speed does not affect mass transfer in laminar flow but causes an exponential mass transfer enhancement in higher turbulent flows. There exists an optimum through-flow rate of the liquid for the best mass transfer performance depending on the initial bubble size and disc speed. Test results [9] provide a qualitative confirmation of the theory.

Introduction

Rotating disc contactors (RDC's) are widely used for gas-liquid absorption and liquid-liquid extraction [1-4]. They are more efficient and flexible in operation than the conventional sieve-plate, packed and spray columns. Howeverm axial mixing tends to decrease the stage efficiency and is always a problem in this type of mixing device. That is why various modifications have been designed to improve efficiency. Figure 1 shows a schematic of a relatively new construction. It consists of a perforated disc rotating in a

vessel comprised of one cylindrical and two conical sections. In gas-liquid mass transfer applications, the liquid flows down by gravity while the gas bubbles rise upward by buoyancy. The perforated rotating disc is used as a dispersing means to reduce the size of gas bubbles and to increase their residence time, resulting in a significant increase in the gas-liquid interface for mass transfer at low power consumption [5]. The housing is designed in a conical shape for the purpose of minimizing the occurrence of axial mixing.

Glaeser et al [6] disclosed that the perforated-disc type devices performed better than propellers and turbines as gas dispersion equipment. Later, Jain [7] studied the power performance and gas holdup of a three-stage perforated-disc cascade in the absence of liquid flow and interphase mass transfer. Experimental results indicated a substantial power reduction that is associated with the presence of the gaseous phase. The physical causes of the large power reduction was explained in reference [8]. Mosch [9] conducted experiments on the same cascade system to determine the effects of gas flow rate and disc rotating speed on the mass transfer coefficient. Reference [5] derived the correlation equation for gas-liquid mass transfer in the mixing cascade using Mosch's data [9].

A series of studies have been conducted to determine the fundamental mechanisms on low power consumption and high interphase mass transfer in the rotating perforated-disc type contactors: The velocity distributions in the axial-swirling combined flow field were determined for both the turbulent [10] and laminar [11] flow cases using a rapidly converging line-relaxation numerical technique. For turbulent flows, a K-ε (turbulent kinetic energy-rate of dissipation energy) two-equation model along with appropriate wall functions were utilized in calculating the turbulent viscosity. The theory provided a basis for the selection of a RDC with a 45-degree conical angle used in the previous experimental studies [5 through 9].

With utilization of the velocity distributions [10, 11] and collaboration of an empirical bubble growth equation, a bubble kinetic equation was numerically integrated to determine the trajectory and velocity of a discrete bubble in the combined flow field [12]. The bubble departed from the center of perforations on the disc rotating at an angular velocity Ω. The Reynolds number based on the hydraulic diameter of the cylindrical section 2 (Ro - Rs) and the Taylor number Ta are defined as

$$Re = \frac{2\dot{m}_\ell}{\pi\mu(R_s+R_o)}, \quad Ta = \frac{\rho\Omega R_d^2}{\mu} \tag{1}$$

Here, $\dot{m}_\ell$ denotes the liquid mass flow rate; μ and ρ, absolute viscosity and density of the liquid, respectively; R_s, R_o and R_d, radii of shaft, cylindrical section, and disc, respectively, as shown in Fig. 1.

The present work is an extension of the previous studies [10 1] to investigate the mass transfer performance between the gas and liquid phases. The effects of Ta, Re and initial bubble size on the performance characteristics of the RDC are determined.

Theoretical Analysis

The physical system to be studied is shown in Fig. 1. The disc is perforated with circular holes at uniform circumferential spacing. A liquid (water) saturated with a dissolved gas (carbon dioxide) enters the contactor from the top opening and flows down along the rotating shaft through the annular space between the disc edge and the cylindrical wall into the lower half of the housing. Gas (air) bubbles are fed into the device through the lower opening. They rise along the shaft by buoyancy, flow radially outward under the lower surface of the rotating disc due to the action of centrifugal and Coriolis forces, and gush through the holes into the upper half of the housing. During the process of passing through the perforations, each bubble is broken up into smaller ones by the shearing action of the solid edges. Due to a combined action of the centrifugal and buoyancy forces, these tiny bubbles travel through the upper half of the housing in counter current with the downpouring liquid. It is during this period of their excursion that the dissolved gas migrates through the liquid toward the bubbles and evaporates into the bubble space. The interphase mass transfer process progresses until gas bubbles are intercepted by a vessel wall. Theoretical analysis is therefore focussed upon the upper half of the flow field.

For convenience in mathematical treatment, the cylindrical coordinates (r, θ, z) are employed with the origin fixed at the center of the disc with z measuring the axial distance in the direction against the liquid flow.

a) Velocity Distribution in the Liquid Phase [10,11]

With the use of the vorticity ω and stream function ψ defined as

$$\omega = \frac{\partial U}{\partial z} - \frac{\partial W}{\partial r} \; ; \; U = \frac{1}{\rho r}\frac{\partial \psi}{\partial z} \; ; \; W = \frac{1}{\rho r}\frac{\partial \psi}{\partial r} \tag{2}$$

the full Navier-stokes equations can be expressed as [10]

$$a\frac{\partial}{\partial z}\left(\phi\frac{\partial \psi}{\partial r}\right) - \frac{\partial}{\partial r}\left(\phi\frac{\partial}{\partial z}\right) - \frac{\partial}{\partial z}\,br\frac{\partial}{\partial z}(c\phi) - \frac{\partial}{\partial r}\,br\frac{\partial}{\partial r}(r\phi) + rd = 0 \tag{3}$$

Here, (U, V, W) denote the velocity components in the (r, θ, z) directions, respectively; ρ, the liquid density; and ϕ, general dependent variable. The coefficients a, b, c and d together with ϕ are listed in Table 1.

TABLE 1: Definition of a, b, c, d and ϕ

ϕ	a	b	c	d
ψ	o	$1/\rho r^2$	1	$-\omega/r$
ω/r	r^2	r^2	$/u_e$	$-\partial(\rho V^2)/\partial z$
κ	1	μ_e/σ_k	1	$\mu_t G - \rho\varepsilon$
ε	1	μ_e/σ_e	1	$C_1\varepsilon\mu_t G/\kappa - C_2\rho\varepsilon^2/\kappa$

Equation (3) can be applied for both laminar and turbulent flows. In case of laminar flows, $\mu_e = \mu$ and only the first three variables in Table 1 are needed; for turbulent flows, all the five equations must be solved. $\mu_e = \mu + \mu_t$, where μ and μ_t are the laminar and turbulent viscosity, respectively. μ_t is defined as $C_D\,\rho\ell K^{1/2}$ which is equal to $\rho\kappa^2 C_u/\varepsilon$. The constants C_1, C_2, C_u, C_D, σ_e and σ_k are 1.45, 2.0, 0.082, 1.0, 1.3 and 1.0, respectively [10]. G signifies the turbulent viscous dissipation function.

The appropriate boundary conditions are

(a) At inlet: $U = V = 0$, $W = f(r)$; (4a)

(b) on stationary walls: $U = V = W = 0$; (4b)

(c) on rotating surfaces: $U = W = 0$, $V = \Omega r$; (4c)

(d) at exit: $U = V = 0$, $\partial W/\partial z = 0$ (4d)

For the near-wall layers where viscous effects predominate over turbulent ones, the "Wall function method" [10] is incorporated in the computer program. A fast-converging line-iterative technique is employed to solve the above equations in finite difference form for the distribution of flow velocities (U, V, W).

(b) Bubble Trajectory and Residence Time in the Reaction Zone [12]

A bubble with diameter less than 3 mm may be treated as a rigid particle [12]. The equation of bubble kinetics can then be found by the balance of the forces acting on a particle (e.g. bubble). Let the components of bubble velocity in the (r, θ, z) direction be expressed in terms of the instantaneous position of the bubble [R(t), Ξ(t), Z(t)]. They are substituted into the force-balanced kinetic equation. It yields

$$\ddot{R} = -\frac{3}{2D_b}(\dot{R} - U)\,\upsilon\,C_d + R\dot{\Xi}^2 + 3\left(U\frac{U}{r} + W\frac{U}{z} - \frac{V^2}{r}\right) \tag{5a}$$

$$\ddot{\Xi} = -\frac{2\dot{R}}{R} - \frac{3}{2D_b R}(R\dot{\Xi} - V)\,\upsilon\,C_d + \frac{I}{R}\left(U\frac{\partial V}{\partial r} + W\frac{\partial V}{\partial z} + \frac{UV}{r}\right) \tag{5b}$$

$$\ddot{Z} = 2g - \frac{3}{2D_b}(\dot{Z} - W)\,\upsilon\,C_d + 3\left(U\frac{\partial W}{\partial r} + W\frac{\partial W}{\partial z}\right) \tag{5c}$$

for the (r, θ, z) direction, respectively. Here, the superscripts "·" and "··" signify the time derivitives. The drag coefficient C_d obeys the relationship [13]:

$$C_d = 4\,(0.75\,Re_b^{0.72} + 6)/\,Re_b \tag{6}$$

Here, Re_b is the bubble Reynolds number defined as $Re_b = D\upsilon/\nu$ and ν signifies the kinematic viscosity of the liquid. υ denotes the relative velocity between the bubble and the surrounding liquid defined as

$$\upsilon = [(U - \dot{R})^2 + (V - R\dot{\Xi})^2 + (W - \dot{Z})^2]^{1/2} \tag{7}$$

wherein $(\dot{R}, R\dot{\Xi}, \dot{Z})$ are the components of bubble velocity in the (r, θ, z) direction, respectively. Equations (5a), (5b), and (5c) are subjected to the initial conditions

$$R(0) = R_h,\ \Xi(0) = 0,\ Z(0) = 0 \tag{8a}$$

$$\dot{R}(0) = 0,\ \dot{\Xi}(0) = \Omega,\ \dot{Z}(0) = 0 \tag{8b}$$

It is assumed that all tiny bubbles produced by the shearing of larger ones by the hole edges are ejected into the liquid region from the center of the holes located at a distance R_h from the shaft axis. The bubble dynamic equation can be derived by combining the mass-transfer rate equation, Henry's law and thermodynamic equation of state for an ideal gas as

$$D_b = D_o \left[1 + \frac{4\bar{R}Th_D}{9HD_o} t\right]^{1/4} \tag{9}$$

where D_o is the initial bubble diameter; H, Henry's constant; $\bar{R}$, universal gas constant; h_D, mass transfer coefficient; T, liquid temperature; and t, time.

Incorporating the liquid velocity distribution together with equations (6), (7) and (9), a fourth-order Runge-Kutta method is utilized to solve equations (5) subject to equations (8) for the instantaneous position and velocity of a bubble. The drag coefficient, liquid velocity and bubble size are updated at every instant. The computions are repeated until the bubble hits a wall.

(c) Interphase Mass Transfer Performance

Let $\dot{n}_a$ be the number of air bubbles ejected from the holes on a rotating disc per unit time. The mass flow rate of the air into the housing is $\dot{m}_a = \dot{n}_a m_a$ wherein m_a is the mass of air inside the bubble of diameter D_o. Each bubble has grown to a final size D_r during the residence time t_r through the migration of carbon dioxide into the bubble space. So, the mass flow rate of the air-CO_2 mixture out from the upper opening of the contactor is $\dot{m}_m = \dot{n}_a m_m$ in which m_m denotes the mass of gas mixture inside the bubble of diameter D_r. The mass rate of the dissolved CO_2 into air bubbles is then

$$\dot{m}_c = \dot{m}_m - \dot{m}_a = \dot{n}_a m_c \quad \text{or} \quad \frac{\dot{m}_c}{\dot{m}_a} = \frac{m_c}{m_a} \tag{10}$$

where $m_c = m_m - m_a$. With application of the thermodynamic equation of state for an ideal gas, the above equation can be approximated as

$$\frac{\dot{m}_c}{\dot{m}_a} = \frac{M_c}{M_a} \left(\frac{D_r}{D_o} \right)^3 - 1 \qquad (11)$$

in which M_c and M_a are the molecular weights of carbon dioxide and gas, respectively. $\dot{V}_c/\dot{V}_a$ represents the ratio of the corresponding volumetric flow rates.

Results and Discussion

For a specified RDC (fixed system geometry as shown in Fig. 1), liquid, dissolved gas and air bubble, the interphase mass transfer performance is controlled by three nondimensional parameters: D_o/R_d, Re and Ta. Here, R_d is 6 cm, while $\bar{R}Th_D/H$ for carbon dioxide in the water-air system is 0.2475 cm/sec at 20 C. Numerical computations were conducted by means of an AMDAHL 470/V7 digital computer with a H compiler.

The parameters were varied as follows: D_o = 1, 2, 3 mm; Re = 174 and Ta = 200 to 600 for laminar flow; and Re = 174 to 1160 with Ta = 5.72×10^4 to 4×10^5 for turbulent flow. Results are graphically presented in Figs. 2 through 5.

Figure 2 illustrates the changes in both the final bubble size in the dimensionless form D_r/D_o and the bubble residence time t_r as a function of the Taylor number. The through-flow Reynolds numbers correspond to 174 and 580 in the laminar and turbulent flow fields, respectively. It is seen in the figure that both D_r and t_r remain constant with Ta for laminar flows with low disc rotation. However, like the recirculating flow strength, they are strongly influenced by Re. In the turbulent flow regime, both D_r and t_r increase with Ta. A reduction in the bubble size results in an increase in D_r/D_o and t_r for both the laminar and turbulent flow cases, as expected. The corresponding mass transfer results are shown in Fig. 3 for the volumetric flow rate ratio $\dot{V}_c/\dot{V}_a$ and mass flow rate ratio $\dot{m}_c/\dot{m}_a$ versus Ta. One observes that the interphase mass transfer of carbon dioxide increases substantially with a reduction in the initial bubble size. The curves for the three different bubble diameters are almost parallel and become steeper as Ta increases. One set of test data at Re = 580 which were obtained by Mosch [9] using a RDC of identical geometry and size as Fig. 1 are superimposed in Fig. 3. Mass transfer rates increase with a decrease in the volumetric flow rate of air through the RDC. A direct comparison between

the test results and the theoretical prediction is not appropriate since in actual operations, it is impossible to measure D_o of air bubbles ejected from the perforations and a good fraction of air bubbles bypasses the holes, entering the upper half RDC through the annular space between the rim of the disc and the cylindrical wall of the housing. However, under the same values of Re and Ta, a higher air flow rate $\dot{V}_a$ would certainly produce a larger D_o of air bubbles. Test results (Re = 98) in Fig. 6 show a similar trend as the theoretical prediction, namely an enhancement in the interphase mass transfer performance with increasing Ta, thus qualitatively supporting the theory.

Figures 4 and 5 deal with the effects of Re on bubble behavior and interphase mass transfer performance, respectively. A reduction in D_o promotes an increase in D_r, t_r and m_c. Re exerts only a limited influence on D_r, t_r and $\dot{m}_c$. An interesting observation is the existence of a maximum value in D_r, t_r and $\dot{m}_c$ at a certain value of Re, approximately 500. This means there exists an optimum liquid flow rate for achieving the best mass transfer performance. A through-flow rate of the liquid either higher or lower than this optimum Re results in a shorter bubble residence time and consequently a lower mass transfer rate. Test results in Fig. 7 correspond to the liquid flow rates lower than the optimum Re. The trend bears out the prediction of the theoretical model.

Conclusions

With the incorporation of equations (6), (7) and (9), numerical integrations of equations (3) and (5) were carried out subject to the boundary conditions (4) and (8). Theoretical results were obtained for the rate of interphase mass transfer of carbon dioxide in the water-air system using equation (11). It is concluded that (i) A reduction in D_o results in a significant enhancement in $\dot{m}_c$ in both laminar and turbulent flow cases. (ii) Ta plays no role on $\dot{m}_c$ in the laminar flow regime. However, in the case of turbulent flow, an increase in Ta promotes an augmentation of $\dot{m}_c$ which increases exponentially with Ta when Ta exceeds 1.5×10^5. (iii) There exists an optimum Re for the best interphase mass transfer performance. $\dot{m}_c$ decreases at a value of Re, either higher or lower than the optimum value. (iv) The theoretical model is in qualitative agreement with the test results.

References

1. P.H. Calderbank, Mixing (ed. by V.W. uhl and J.B. Gray), Vol. II Academic Press, New York, Chap. 6 (1966).

2. G.S. Laddha and T.F. Degaleesan, Transport phenomena in liquid extraction, McGraw-Hill, New York (1978).

3. G.H. Reman and R.B. Olney, Chem. Eng. Progress 51, 141 (1955).

4. F. Yoshida and Y. Miura, Ind. & Eng. Chem., Process Design Development 2, 263 (1963).

5. Wen-Jei Yang, Mechanism of power dissipation in liquid-gas mixing in a perforated-disk type stirring cascade, Heat Transfer 1978, Vol. 4 Hemisphere, Washington, D.C., 7 (1978).

6. H. Glaeser, B.O. Biesecker and H. Brauer, H. Verferenstechnik, 2,31 (1973).

7. S.H. Jain, Einfluss geneigter Strombrecher auf die Flussigkeitsbegasung in einem Mehrphasenruhrreaktor, Studienarbeit Matr.-Nr. A4219, Technische Universitat Berlin (1973).

8. Wen-Jei Yang, Letters J. Heat and Mass Transfer 3, 403 (1976).

9. J. Mosch, Experimentelle Untersuchung des Flussigkeitsseitig Kontrollierten Stoff-Ubergangs in Einer mehrstufigen Ruhrkaskade, Institut fur Chem-eingenieurtechnik, Technische Universitat Berlin, Matr.-Nr. 41 449 (1976).

10. J.H. Wang and Wen-Jei Yang, Numerical Methods for Nonlinear Problems (ed. by C. Taylor, E. Hinton and D.R.J. Owen), Vol. 1, Pineridge Press, Swansea, U.K., 885 (1980).

11. J.H. Wang and Wen-Jei Yang, Numerical Methods in Laminar and Turbulent Flow (ed. by C. Taylor and B.A. Schrefler), Pineridge Press, Swansea, U.K., 129 (1981).

12. J.H. Wang and Wen-Jei Yang, H. Non-Equilibrium Thermodynamics 5, 217 (1980).

13. B.E. Launder and D.B. Spalding, Computer Methods in Applied Mechanics and Engineering, Vol. 3, 269 (1974).

14. V.G. Levich, Physicochemical Hydrodynamics, Prentice Hall, Englewood Cliff, NJ. (1962).

15. F. Odar, Verification of the proposed equation for calculation of the forces on a sphere accelerating in a viscous fluid, USA Army CRREL RR, 190 (1966).

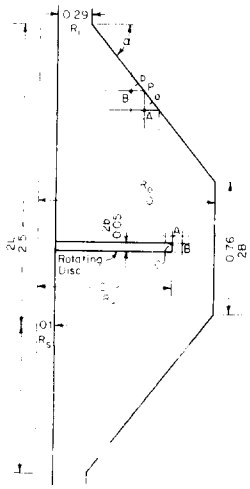

Fig.1 A schematic of disc-type contactor and numerical grid (R_o=79.4 mm)

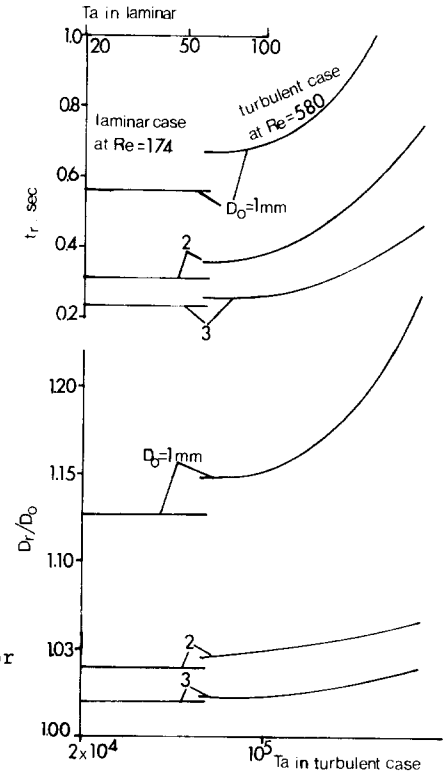

Fig.2 D_r/D_o and t_r versus Ta

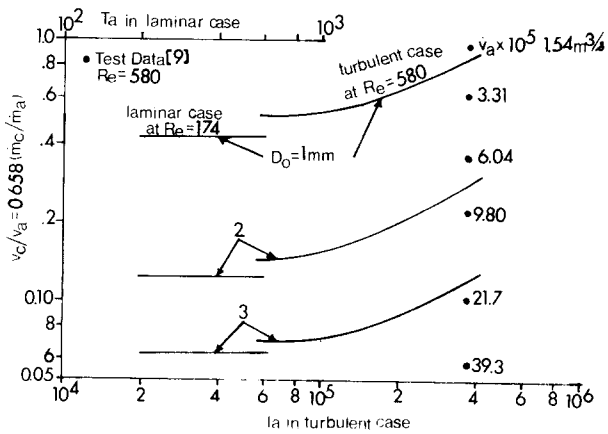

Fig.3 Theoretical results indicating the effects of D_o and Ta interphase mass transfer of CO_2 in water-air system

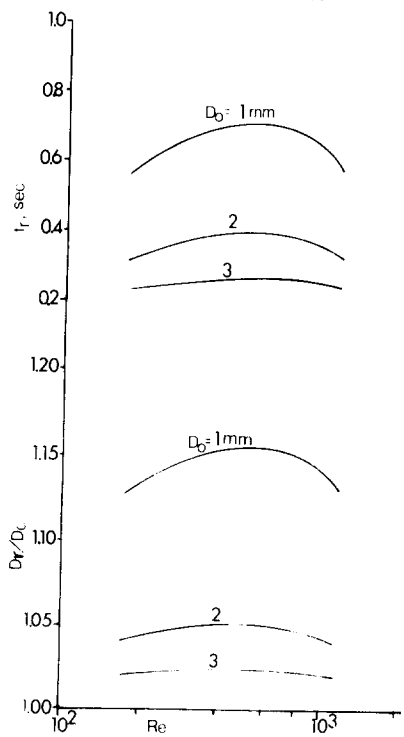

Fig.4 D_r/D_o and t_r versus Re

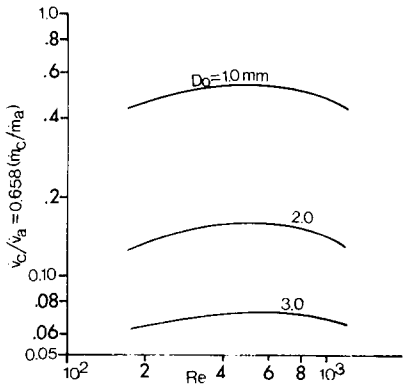

Fig.5 Theoretical results indicating the effects of Re on interphase mass transfer of CO_2 in water-air system at Ta = 1.14×10^5

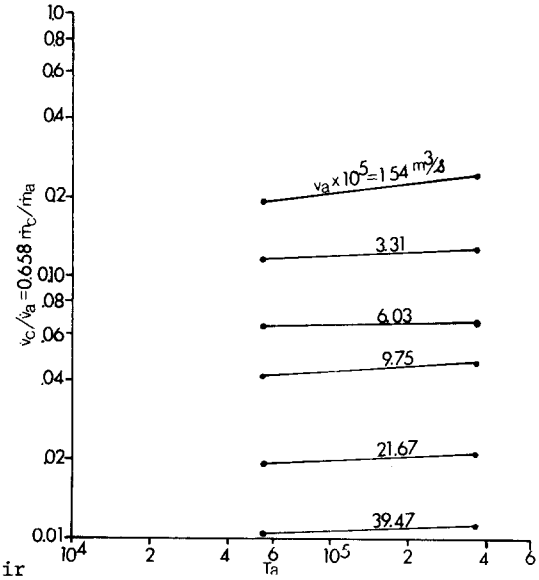

Fig.6 Experimental results for the effects of Ta and $\dot{V}_a$ on interphase mass transfer of CO_2 in water-air system at Re = 98[9]

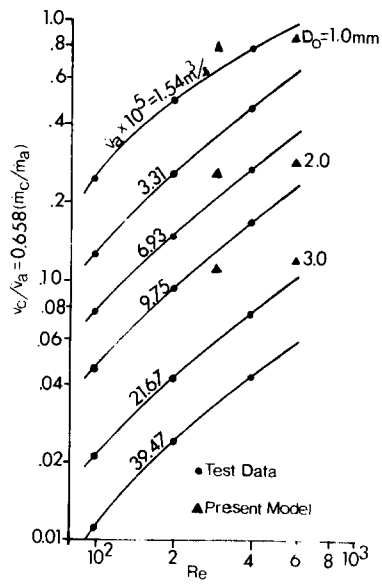

Fig.7 Experimental results for the effects of Re on interphase mass transfer of CO_2 in water-air system at Ta = 3.65×10^5[9]